Journal of Magnetic Resonance **138,** 281–287 (1999)
Article ID jmre.1999.1753, available online at http://www.idealibrary.com on IDEAL®

"BEST" Homonuclear Adiabatic Decoupling for ^{13}C- and ^{15}N-Double-Labeled Proteins

Shanmin Zhang and David G. Gorenstein

Sealy Center for Structural Biology and the Department of Human Biological Chemistry and Genetics, University of Texas Medical Branch, Galveston, Texas 77555-1157

Received December 18, 1998; revised March 3, 1999

The cyclic irradiation sidebands appearing in homonuclear adiabatic decoupling are calculated in detail, which reveals the origin of the antisymmetric sidebands. The sidebands can be inverted by inserting an initial decoupling with a different period, but the same f_{1rms} as the main decoupling that is required for Bloch–Siegert shift compensation. The sidebands can be eliminated in a broad decoupling range by adding spectra of opposite sidebands. Based on this scheme, an offset-independent double-adiabatic decoupling, named Bloch–Siegert Shift Eliminated and Cyclic Sideband Trimmed Double-Adiabatic Decoupling, or "BEST" decoupling for short, is constructed, which not only compensates the Bloch–Siegert shift as shown earlier by Zhang and Gorenstein (1998) but also eliminates residual sidebands effectively.

INTRODUCTION

Homonuclear decoupling has been used intensively in triple-resonance multidimensional NMR (*1–3*), especially for ^{13}CO–$^{13}C_\alpha$ decoupling for ^{13}C- and ^{15}N-double-labeled proteins. As in other applications, it simplifies the spectrum and enhances the signal-to-noise ratio (*4*). To minimize disturbances of nearby NMR peaks, homonuclear decoupling requires a decoupling profile of sharp edges. One of the best decoupling schemes is adiabatic decoupling (*5–9*). Not only does it have an ideal decoupling profile for homonuclear decoupling (*10, 11*), but it also has the highest ratio of decoupling range divided by the root-mean-square value of the RF field strength, f_{1rms}, which in turn minimizes sample heating.

As in heteronuclear adiabatic decoupling (*12–16*), homonuclear adiabatic decoupling also introduces significant sidebands due mainly to a long decoupling period compared with the inverse of sampling rate or dwell time. The origin of the sidebands is, however, different. In heteronuclear adiabatic decoupling, the sidebands, often referred to as decoupling sidebands, are created by the periodic modulation of coupling by the RF field. In homonuclear, ^{13}CO–$^{13}C_\alpha$ decoupling, for example, the sidebands, termed cyclic irradiation sidebands, are introduced mainly by direct irradiation of the decoupling RF field, while the effect of the modulation of the coupling is quite small because of small ^{13}CO–$^{13}C_\alpha$ coupling constant (*17, 18*).

Unlike heteronuclear decoupling, homonuclear decoupling inevitably introduces frequency shifts of all peaks, as discovered by Bloch and Siegert (*19*). The amount of the Bloch–Siegert shift depends on f_{1rms} of the decoupling field and the frequency difference between the NMR peak and the decoupling carrier frequency (*18–24*).

The Bloch–Siegert shift was reduced partially by McCoy and Mueller (*23*) with a compensating field situated on the other side of the NMR peaks. Unfortunately, it only eliminates completely the Bloch–Siegert shift for the central (midpoint of the decoupling and compensating pulses) point. A reduced offset-dependent Bloch–Siegert shift still remains, which can be experimentally problematic, especially at very high magnetic fields. Recently, we have introduced a double-adiabatic decoupling (*18*), which causes a spectrum contraction by a factor of $\lambda = [1 - (f_{1rms}/\Delta f)^2]$, where f_{1rms} is the root-mean-square value of the decoupling field and Δf is one-half of the frequency difference between the two decoupling pulses. The spectrum contraction, by nature, is the Bloch–Siegert shift introduced by two nearby decoupling fields, and it can be compensated in a quite broad decoupling range by a dilated evolution time $t_1' = [1 + (f_{1rms}/\Delta f)^2]t_1$ (*18*). Besides, this double-adiabatic decoupling also reduces significantly the cyclic irradiation sidebands, especially for peaks in the central region of the spectrum. For large offset, ± 3 kHz for example, there are about 2% residual sidebands with sideband number $n = \pm 1$. Also, the decoupling sidebands will not be reduced by the compensating pulse, which is far off-resonance to the coupled spins.

To eliminate the residual sidebands and to compensate the Bloch–Siegert shift, a constant f_{1rms} during decoupling is required; otherwise, the Bloch–Siegert shift in the frequency domain will not be easily predicted. This prevents the use of many schemes in heteronuclear adiabatic decoupling for eliminating sidebands, such as the bilevel adiabatic decoupling (*13*) and the adiabatic *R*-variation (*25*).

In this contribution, the origin of the antisymmetric sidebands and their amplitudes are discussed in detail. The inver-

1090-7807/99 $30.00

sion of the sidebands by insertion of an initial decoupling with the same f_{1rms} as the main decoupling is then introduced, and finally this scheme is adapted for double-adiabatic decoupling (*18*), referred to as Bloch–Siegert Shift Eliminated and Cyclic Sideband Trimmed Double-Adiabatic Decoupling, or "BEST" decoupling for short.

CYCLIC IRRADIATION SIDEBANDS

As demonstrated earlier (*17*, *18*), the cyclic irradiation sidebands are introduced by the irradiation of a cyclic decoupling field near a NMR line. The decoupling field creates not only the sidebands but also a Bloch–Siegert shift. It was shown that both the sidebands and the Bloch–Siegert shift were caused mainly by a time-dependent first-order average Hamiltonian in the rotating frame (*18*),

$$\bar{\mathcal{H}}^{(1)}(t) = -\frac{f_{1rms}^2(t)}{2\Delta f_1} I_z = -\left[\frac{f_{1rms}^2(t) - f_{1rms}^2}{2\Delta f_1} I_z\right] - \frac{f_{1rms}^2}{2\Delta f_1} I_z = H(t) - \frac{f_{1rms}^2}{2\Delta f_1} I_z, \quad [1]$$

where $f_{1rms}(t)$, defined as

$$f_{1rms}(t) = \sqrt{\frac{1}{t}\int_0^t f_1^2(t')dt'} \quad [2a]$$

and

$$f_{1rms}(T) = f_{1rms}, \quad [2b]$$

is a time-dependent root-mean-square value of the RF field $f_1(t)$, and Δf_1 is the decoupling carrier frequency minus NMR peak frequency. The second term on the right side of Eq. [1], which introduces a Bloch–Siegert shift, can be removed by introducing a second rotating frame (*26*, *27*) with a rotating frequency equal to the Bloch–Siegert shift, i.e., $\omega_r/2\pi = |f_{1rms}^2/2\Delta f_1|$. We call this particular second rotating frame the Bloch–Siegert rotating frame. In the Bloch–Siegert rotating frame, the first-order average Hamiltonian reduces to

$$\bar{\mathcal{H}}_{BS}^{(1)}(t) = -\left[\frac{f_{1rms}^2(t) - f_{1rms}^2}{2\Delta f_1} I_z\right] = H(t), \quad [3]$$

which is periodic with a period of T and $H(nT) = 0$.

In the Bloch–Siegert rotating frame the Bloch–Siegert shift term disappears, but a periodic interaction (Eq. [3]) remains. Therefore, the spins will precess with their own frequency on average and the precession is phase modulated by the periodic interaction. It is this periodic phase modulation that results in the cyclic irradiation sidebands.

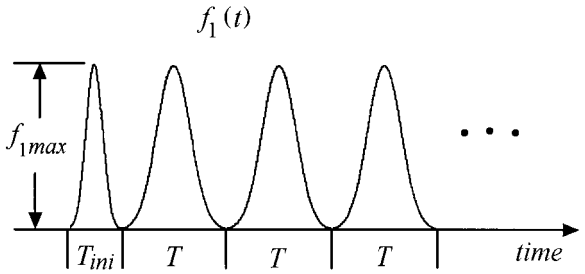

FIG. 1. Gaussian-shaped adiabatic decoupling with an initial decoupling period T_{ini} and the main decoupling period T. As T_{ini} varies, the phases of sidebands will change accordingly while the phase of the central peak remains unchanged. In particular, the sidebands ($n = \pm 1$) are inverted if $T_{ini} = T/2$.

The periodic phase modulation can be calculated easily:

$$\vartheta(t) = 2\pi[H(t)/I_z]t. \quad [4]$$

If the shape of the decoupling pulse is symmetric with respect to the middle point of a period T, i.e.,

$$f_1\left(\frac{T}{2} - t\right) = f_1\left(\frac{T}{2} + t\right), \quad 0 \le t \le T/2, \quad [5]$$

from Eqs. [2]–[5], it is easy to derive that

$$f_{1rms}^2(T/2) = f_{1rms}^2(T) \quad [6]$$

and

$$H(T/2) = 0 \quad [7a]$$

$$\vartheta(T/2) = 0. \quad [7b]$$

It can be further shown that the phase modulation is antisymmetric with respect to the middle point,

$$\vartheta\left(\frac{T}{2} - t\right) = -\vartheta\left(\frac{T}{2} + t\right), \quad 0 \le t \le T/2. \quad [8]$$

A phase modulation, created by a Gaussian shaped pulse (with $T_{ini} = 0$), is shown in Fig. 1. Since a Gaussian shape is symmetric, the phase modulation appears to be antisymmetric with respect to the middle point of the period as expected. It is this antisymmetric phase modulation, which resembles a sine function, that creates antisymmetric sidebands.

The $FID(t)$ in the Bloch–Siegert rotating frame is then the original FID (without the decoupling pulse), defined as $g(t)$, times the phase modulation,

$$FID(t) = g(t) \times [\cos(\vartheta(t)) + i \sin(\vartheta(t))]. \quad [9]$$

For small $\vartheta(t)$, which corresponds to a low RF decoupling and

TABLE 1
Amplitudes of Cyclic Sidebands for a Gaussian-Shaped Decoupling Scheme

Sideband number	$n = -2$	-1	0	1	2
Observed	−0.014	0.073	0.995	−0.068	0.016
Calculated	−0.015	0.071	0.995	−0.069	0.019

is always the case in homonuclear decoupling, Eq. [9] reduces to

$$FID(t) \approx g(t) \times [(1 - \vartheta^2(t)/2) + i\vartheta(t)]. \quad [10]$$

The NMR line in the Bloch–Siegert rotating frame can be expressed as

$$FT\{FID(t)\} = FT\{g(t)\} * FT\{(1 - \vartheta^2(t)/2) + i\vartheta(t)\}, \quad [11]$$

where $FT\{g(t)\}$ is the original line and $FT\{i\vartheta(t)\}$ contributes to discrete antiphase sideband amplitudes, while $FT\{(-\vartheta^2(t)/2)\}$ contributes to discrete small symmetrical sideband amplitudes.

The relative amplitudes of the sidebands can be obtained by calculating the Fourier coefficients,

$$A_n = \frac{1}{T}\int_0^T [(1 - \vartheta^2(t)/2) + i\vartheta(t)]e^{i(n2\pi t/T)}dt. \quad [12]$$

The amplitudes of the cyclic irradiation sidebands for $n = -2$ to 2 together with the observed results are shown in Table 1. Here $\vartheta(t)$ is obtained using Eq. [4] with the parameters shown in Fig. 2, and the experimental results are obtained with the same conditions. The central peak from the experiment is normalized to the calculated value. The positive sidebands are slightly higher than their counterpart negative sidebands. This is caused partly by the term $FT\{(-\vartheta^2(t)/2)\}$, which creates small positive sidebands that are added to the antisymmetric sidebands. Since the small positive sidebands contribute to the integral of the peak, they will reduce the amplitude of the central peak slightly. Similar to heteronuclear decoupling, homonuclear decoupling will also introduce decoupling sidebands, which will also be added to the main antisymmetrical sidebands.

Disregarding the small symmetric contribution, one obtains antisymmetric sidebands,

$$A_n = -A_{-n}. \quad [13]$$

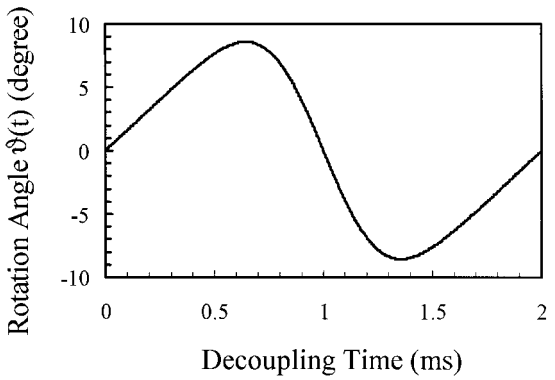

FIG. 2. A period of phase modulation of transverse magnetization in the Bloch–Siegert rotating frame created by a Gaussian-shaped decoupling pulse, $A(t) = f_{1max}\exp[-\alpha(t - T/2)^2]$ with $\alpha = 5$ (kHz)^2, $T = 2$ ms, $f_{1max} = 2.72$ kHz, and $f_{1rms} = 1.44$ kHz, located 23.2 kHz higher than the NMR peak frequency.

Further, all the A_n are real because of the symmetry of $\vartheta(t)$ as shown in Eq. [8]. Also, since $\vartheta(t) \propto [f_{1rms}^2(t) - f_{1rms}^2]$ and both $f_{1rms}^2(t)$ and $f_{1rms}^2 \propto f_{1max}^2$, one gets $\vartheta(t) \propto f_{1max}^2$. It follows that

$$|A_n| \propto f_{1max}^2 \propto f_{1rms}^2, \quad [14]$$

which agrees well with the calculated results shown in Fig. 3. Similarly, one can see from Eqs. [3] and [4] that $|A_n|$ is inversely proportional to Δf_1.

The field dependence of the amplitudes of the cyclic irradiation sidebands can be understood by the following analysis. As the external magnetic field increases, the decoupling range and Δf_1 increase linearly, while the decoupling power or f_{1rms}

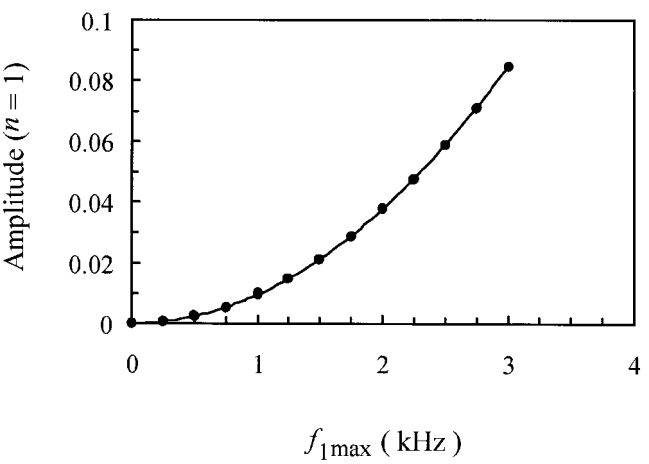

FIG. 3. Amplitudes $|A_n|$ of cyclic irradiation sidebands for $n = 1$ as a function of $f_{1max}(=1.89\ f_{1rms})$ (solid circles), calculated with Eqs. [2]–[4], and [12]. The solid curve is a function of $|A_n| = \lambda f_{1max}^2$ (or $|A_n| \propto f_{1max}^2 \propto f_{1rms}^2$), where λ is a constant and is defined in such a way that the solid circle and curve match at $f_{1max} = 1.5$ kHz.

increases as a function of the square root of the decoupling range for adiabatic decoupling (*8, 12*). It turns out that $|A_n|(\propto f_{1rms}^2/\Delta f_1)$ is independent of magnetic field for adiabatic decoupling. For other decoupling schemes with a decoupling index <2 (*12*), however, the sideband amplitudes will increase as field increases.

INVERSION OF THE CYCLIC IRRADIATION SIDEBANDS

One of the effective ways to cancel the sidebands is to invert them, followed by adding the two FIDs. This can be accomplished in heteronuclear decoupling either by delaying the initial sampling with a spin echo as demonstrated by Kupče (*15*), or by using a bilevel decoupling with a strong initial decoupling pulse as shown by Kupče *et al.* (*13*). Both methods work quite well in heteronuclear decoupling under certain conditions. However, the spin echo method suffers signal loss of the magnetization due to spin–spin relaxation. The bilevel decoupling will disturb the magnetization of interest that is not too far away from the decoupling pulse and will cause an unpredictable Bloch–Siegert shift.

To invert the sidebands with $n = \pm 1$, one can simply insert an initial decoupling of half period as the main decoupling, i.e., $T_{ini} = T/2$ (Fig. 1). However, this initial decoupling pulse must have the same f_{1rms} as the main decoupling in order to compensate the Bloch–Siegert shift (*18*). Also, it is necessary to have the same inversion band as the main decoupling pulse.

In our experiments, a Gaussian-shaped pulse,

$$A(t) = f_{1max}\exp[-\alpha(t - T/2)^2], \qquad [15]$$

is used. The frequency-independent adiabatic inversion (*10, 16*) is constructed according to Ref. *16*. The initial decoupling also has a Gaussian shape, with the same amplitude f_{1max} and the same inversion bandwidth as the main decoupling pulse (Fig. 1). It has a period of $T_{ini} = T/2$ and

$$\alpha_{ini} = \alpha\left(\frac{T}{T_{ini}}\right)^2. \qquad [16]$$

Equation [16] ensures that both the initial and the main decoupling have the same cutoff amplitude at the beginning, $A_{ini}(0) = A(0)$, and at the end, $A_{ini}(T) = A(T)$, of a period. The cutoff amplitude in our case is about 0.7% of the peak value.

It is important to note that this initial Gaussian decoupling has an rms value of RF field $f_{1inirms}$ equal to that of the main decoupling, which is exactly needed for Bloch–Siegert shift compensation. This characteristic is shown in the following. According to the definition of the rms value,

$$\begin{aligned} f_{1inirms}^2 &= \frac{1}{T_{ini}}\int_0^{T_{ini}} A_{ini}^2(t)dt = \frac{f_{1max}^2}{T_{ini}}\int_0^{T_{ini}} \\ &\quad \times \exp\left[-\alpha_{ini}\left(t - \frac{T_{ini}}{2}\right)^2\right]^2 dt \\ &= \frac{f_{1max}^2}{T_{ini}}\int_0^{T_{ini}} \exp\left[-\alpha\left(\frac{tT}{T_{ini}} - \frac{T}{2}\right)^2\right]^2 dt, \end{aligned} \qquad [17]$$

where Eq. [16] has been used. A new variable $u = tT/T_{ini}$ can be inserted in Eq. [17], resulting in

$$f_{1inirms}^2 = \frac{f_{1max}^2}{T}\int_0^{T} \exp[-\alpha(u - T/2)^2]^2 du = f_{1rms}^2. \qquad [18]$$

Since no assumption is made about T_{ini} in the above derivation, the relation (Eq. [18]) is true for any T_{ini} as long as Eq. [16] holds.

Equation [18] shows that all the Gaussian decoupling sequences constructed with the relationship of Eq. [16] will have the same f_{1rms} and therefore have the same contribution to the Bloch–Siegert shift.

Under the two-stage decoupling, the $FID(t)$ is modulated as

$$FID(t) = \begin{cases} g(t) \times [1 + i\vartheta_{ini}(t)], & \text{for } 0 \le t < T_{ini} = T/2, \quad [19a] \\ g(t) \times \left[1 + i\,\vartheta\left(t - \frac{T}{2}\right)\right], & \text{for } T/2 \le t, \quad [19b] \end{cases}$$

where the small contributions from $\vartheta_{ini}^2(t)$ and $\vartheta^2(t)$ are neglected for simplicity. $\vartheta_{ini}(t)$ is created by the initial decoupling pulse and has a period of $T_{ini} = T/2$, while $\vartheta(t)$ is created by the main decoupling pulse and has a period of T. Equations [19a] and [19b] can be considered as two *FID*s,

$$FID_1(t) = g(t) \times \left[1 + i\,\vartheta\left(t + \frac{T}{2}\right)\right], \quad \text{for} \quad 0 \le t, \qquad [20a]$$

and

$$FID_2(t) = \begin{cases} g(t) \times \left\{1 + i\left[\vartheta_{ini}(t) - \vartheta\left(t + \frac{T}{2}\right)\right]\right\}, & \text{for } 0 \le t < T/2, \\ 0, & T/2 \le t. \end{cases} \quad [20b]$$

$FID_1(t)$ differs from the original $FID(t)$ (Eq. [11]) in that the modulation $\vartheta(t)$ has a time shift of half period $T/2$, which corresponds to a phase shift in the frequency domain, i.e.,

$$FT\{i\varphi(t + T/2)\} = e^{-i(\omega T/2)} FT\{i\varphi(t)\}, \quad [21]$$

where $\omega = n2\pi/T$. It follows that

$$e^{-i(\omega T/2)} = e^{-i(n\pi)} = \begin{cases} -1, & \text{for odd } |n| \\ 1, & \text{for even } |n| \end{cases}. \quad [22]$$

Correspondingly, all the sidebands with odd number $|n|$ are inverted while the others remain unchanged.

Similarly, if $T_{ini} = T/4$ all the sidebands are inverted with a sideband number $n = \pm 2, \pm 6, \pm 10, \ldots$, while a phase shift $\theta = -n\pi/2$ is introduced for other n. If $T_{ini} = 3T/4$, all the sidebands are inverted with a sideband number $n = \pm 2, \pm 6, \pm 10, \ldots$, while a phase shift $\theta = -n3\pi/2$ is introduced for other n. Practically, it is often sufficient to eliminate only the sidebands with $n = \pm 1$ and ± 2. In this case only four experiments are necessary with $T_{ini} = 0$, $T/4$, $T/2$, and $3T/4$. Adding up all the four experiments cancels the sidebands (Fig. 4). Indeed, only two experiments are required to eliminate the large main sidebands with $n = \pm 1$.

The $FID_2(t)$ (Eq. [20b]), which is nonzero only in the initial period of $T/2$, will create a spectrum spread over a range of $4/T$ and has an amplitude approximately $T/2T_{acq}$ of the sideband amplitude ($n = 1$), where T_{acq} is the acquisition time in t_1 dimension. This small disturbance can be neglected as long as $T_{acq} \gg T$, which is always the case practically.

EXPERIMENTAL

In all the experiments, a ^{15}N- and ^{13}C-labeled (-COOH is unlabeled) *N*-acetylglycine (Fig. 4) is used with a gradient version of HSQC (*28*). During the $^{13}CH_3$ evolution (t_1) time a homonuclear decoupling at ^{13}CO is applied with a frequency shifted excitation (*27, 18*). All the decoupling pulses have a Gaussian shape $A(t) = f_{1max}\exp[-\alpha(t - T/2)^2]$. Gaussian adiabatic decoupling gives the quite sharp decoupling profile that is desired for homonuclear decoupling, and it is easy to construct an f_{1rms} invariant decoupling with different periods but nearly the same decoupling width. However, other shaped pulses could equally be utilized. The main decoupling has $\alpha =$ 5 (kHz)^2, $T = 2$ ms, $f_{1max} = 2.72$ kHz, and $f_{1rms} = 1.44$ kHz. The RF power level is increased 6 dB for the "BEST" decoupling, which corresponds to double the amplitude. The f_{1rms} and the RF power, however, have been increased only by a factor of $\sqrt{2}$ and 2, respectively, because of the interference of the two decoupling pulses. The offset-independent adiabatic decoupling is constructed according to Ref. (*16*) with an 8-kHz frequency sweep and a phase cycle of (0°, 150°, 60°, 150°, 60°) (*29, 30*). The initial decoupling period is constructed according to Eq. [16]. All the experiments were performed on a 600-MHz Varian Unit Plus NMR instrument with a Varian 5-mm HCN triple-resonance probe.

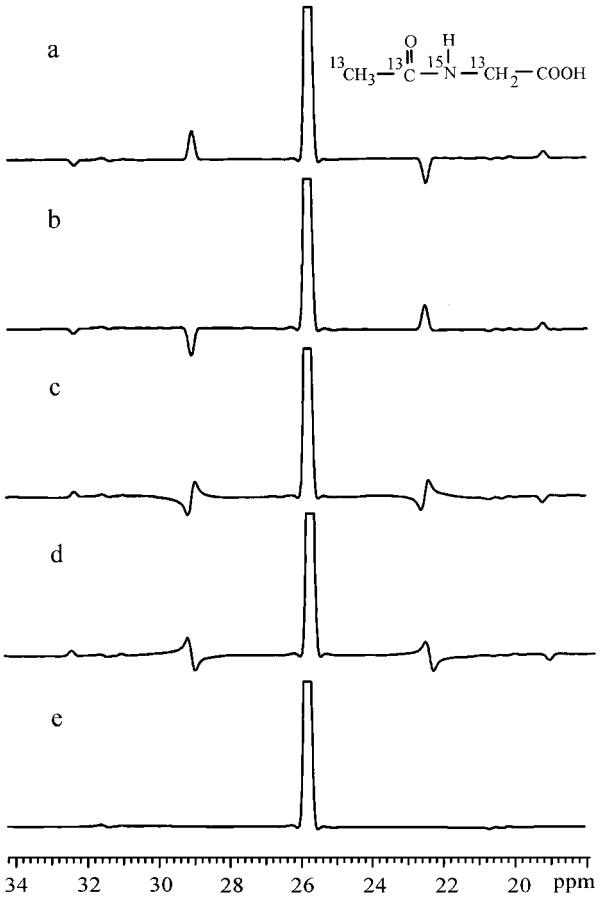

FIG. 4. Methyl ^{13}C spectra from the traces of two-dimensional HSQC spectra using a sample of double-labeled *N*-acetylglycine. The spectra are obtained using the decoupling sequence shown in Fig. 1, with $T_{ini} = 0$ (a), $T_{ini} = T/2$ (b), $T_{ini} = T/4$ (c), and $T_{ini} = 3T/4$ (d). Spectrum (e) is the sum of the four (a to d) spectra. The central peak is truncated at 40% level.

The ^{13}C traces from HSQC spectra are shown in Fig. 4, obtained using the decoupling scheme shown in Fig. 1, with different T_{ini}. Figure 4a is obtained with $T_{ini} = 0$, which shows a normal spectrum under homonuclear decoupling with a Bloch–Siegert shift of 45.0 Hz. The sidebands appear to be antisymmetric because of the antisymmetric phase modulation (Fig. 2) as discussed above. The sidebands will also be inverted

if the decoupling pulse moves from one side of the NMR peak to the other as demonstrated and explained earlier (*18*). Figure 4b shows the spectrum with $T_{ini} = T/2$. The sidebands with $n = \pm 1$ are inverted, but the sidebands $n = \pm 2$ remain unchanged as theory predicts. Therefore, the sidebands ($n = \pm 1$) can be eliminated by adding Figs. 4a and 4b. This will be sufficient for most applications, since the remaining sidebands are quite small. The spectra for initial decoupling period $T_{ini} = T/4$ and $3T/4$ are shown in Figs. 4c and 4d, respectively. Now, the sidebands with $n = \pm 2$ are inverted but the sidebands with $n = \pm 1$ have $\mp 90°$ (Fig. 4c) and $\mp 270°$ (Fig. 4d) phase shifts, as also predicted. By adding all four spectra (Figs. 4a to 4d), all the sidebands with $n = \pm 1$ and ± 2 are entirely eliminated as shown in Fig. 4e.

For $T_{ini} = T/4 = 0.5$ ms initial decoupling, the inversion profile may degrade because T_{ini} is too small. To avoid this problem, two decoupling periods, one with $T_{ini} = 1.0$ ms and the other 1.5 ms, are used. The total initial decoupling time is then 2.5 ms. Since it is 2 ms (a single period) longer than $T/4$, it will give the same phase shift as $T_{ini} = T/4$.

The irradiation sidebands can also be reduced significantly by a double-adiabatic homonuclear decoupling used to compensate Bloch–Siegert shift (*18*). It is quite effective for small offsets. For a large offset, ± 3 kHz, for example, residual sidebands are about 2% with $n = \pm 1$ and negligibly small for the rest of the sidebands. The double-adiabatic decoupling, however, has no effect on the decoupling sidebands.

By inserting an initial double-adiabatic decoupling period $T_{ini}(=T/2)$ into the double-adiabatic decoupling (*18*), the residual sidebands with $n = \pm 1$ will also be inverted and therefore can be eliminated. Since the initial double-adiabatic decoupling has the same f_{1rms} as the main double-adiabatic decoupling, the Bloch–Siegert shift can be eliminated with a dilated evolution time as demonstrated recently (*18*). As mentioned above, we call this particular double-adiabatic decoupling the "BEST" decoupling.

The experimental results obtained with this BEST decoupling are shown in Fig. 5. For $T_{ini} = 0$, an antisymmetric residual sidebands ($n = \pm 1$) appears in Fig. 5a and the sidebands are inverted with an initial decoupling $T_{ini} = T/2$ as shown in Fig. 5b. When these two spectra are added, the residual sidebands with $n = \pm 1$ are cancelled as shown in Fig. 5c.

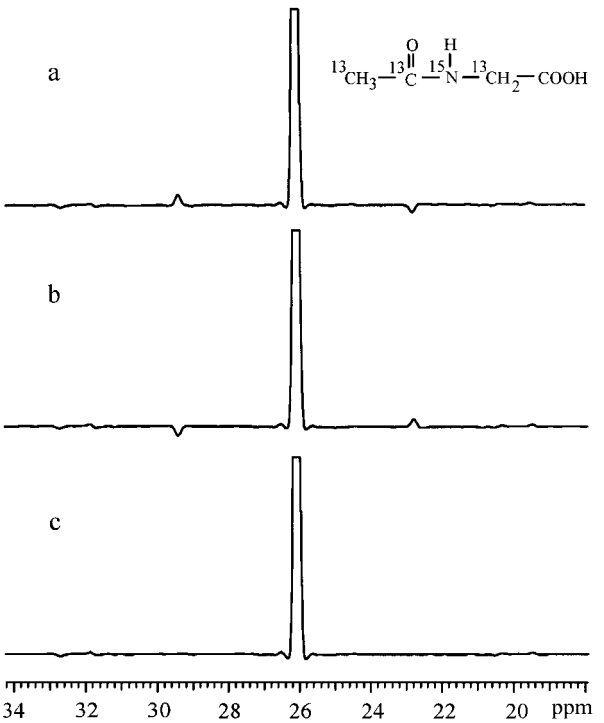

FIG. 5. Methyl ^{13}C spectra from the traces of two-dimensional HSQC spectra using a sample of double-labeled *N*-acetylglycine. The spectra are obtained using "BEST" decoupling, with a ^{13}C decoupling offset of -2.5 kHz and $T_{ini} = 0$ (a) and $T_{ini} = T/2$ (b). Spectrum (c) is the sum of spectra (a) and (b). The central peak is truncated at 40% level.

CONCLUSIONS

In homonuclear decoupling, the antisymmetric sidebands are caused by an antisymmetric phase modulation in the Bloch–Siegert rotating frame. The phase modulation results from the direct cyclic irradiation of a nearby decoupling field. Unlike the symmetric sidebands observed in most heteronuclear decoupling, the antisymmetric sidebands make no contribution to peak integration since the counter parts cancel. Therefore, they will not reduce the intensity of the central peak. The sideband amplitudes $|A_n|$ are proportional to f_{1rms}^2 and inversely proportional to the frequency difference between the peak and the decoupling carrier frequency. Also, $|A_n|$ are independent of magnetic field for adiabatic decoupling. But for other decoupling schemes, they increase as magnetic field increases. The sidebands can be eliminated by inserting an initial decoupling with the same f_{1rms} as the main decoupling pulse. This scheme can be implemented in the double-adiabatic decoupling (*18*) to construct the BEST decoupling, which eliminates not only the Bloch–Siegert shift but also the residual sidebands.

The scheme, inserting an initial decoupling, can also be used in heteronuclear adiabatic decoupling to eliminate sidebands (S. Zhang and D. G. Gorenstein, unpublished). More importantly, it also eliminates the subharmonic decoupling sidebands (*14, 15*) without requiring an echo delay, which may reduce the observed magnetization in spins with short spin–spin relaxation times. The details of the application of this method to heteronuclear decoupling will be discussed elsewhere.

ACKNOWLEDGMENTS

This research was supported by NIH (AI27744), NIEHS (ES06676), the Welch Foundation (H-1296), the Lucille P. Markey Foundation, and the Sealy and Smith Foundation. Building funds were provided by NIH (1CO6CA59098).

REFERENCES

1. L. E. Kay, M. Ikura, R. Tschudin, and A. Bax, *J. Magn. Reson.* **89,** 496 (1990).
2. D. R. Muhandiram and L. E. Kay, *J. Magn. Reson. B* **103,** 203 (1994).
3. L. E. Kay, G. Y. Xu, and T. Yamazaki, *J. Magn. Reson. A* **109,** 129 (1994).
4. R. R. Ernst, G. Bodenhausen, and A. Wokaun, "Principles of Nuclear Magnetic Resonance in One and Two Dimensions," Clarendon Press, Oxford (1987).
5. M. S. Silver, R. I. Joseph, C.-N. Chen, V. J. Sank, and D. I. Hoult, *Nature* **310,** 681 (1984).
6. J. Baum, R. Tyko, and A. Pines, *Phys. Rev. A* **32,** 3435 (1985).
7. M. R. Bendall, *J. Magn. Reson. A* **112,** 126 (1995).
8. Ē. Kupče and R. Freeman, *J. Magn. Reson. A* **115,** 273 (1995).
9. R. Fu and G. Bodenhausen, *J. Magn. Reson. A* **117,** 324 (1995).
10. Ē. Kupče and G. Wagner, *J. Magn. Reson. B* **109,** 329 (1995).
11. H. Matsuo, Ē. Kupče, H. Li, and G. Wagner, *J. Magn. Reson. B* **113,** 91 (1995).
12. S. Zhang, J. Wu, and and D. G. Gorenstein, *J. Magn. Reson. A* **123,** 181 (1996).
13. Ē. Kupče, R. Freeman, G. Wider, and K. Wüthrich, *J. Magn. Reson. A* **122,** 81 (1996).
14. Ē. Kupče and R. Freeman, *J. Magn. Reson.* **127,** 36 (1997).
15. Ē. Kupče, *J. Magn. Reson.* **129,** 219 (1997).
16. A. Tannús and M. Garwood, *J. Magn. Reson. A* **120,** 133 (1996).
17. J. Weigelt, A. Hammarström, W. Bermel, and G. Otting, *J. Magn. Reson. B* **110,** 219 (1996).
18. S. Zhang and D. G. Gorenstein, *J. Magn. Reson.* **132,** 81 (1998).
19. F. Bloch and A. Siegert, *Phys. Rev.* **57,** 552 (1940).
20. W. S. Warren, *J. Chem. Phys.* **81,** 5437 (1984).
21. L. Emsley and G. Bodenhausen, *Chem. Phys. Lett.* **168,** 297 (1990).
22. S. Grzesiek and A. Bax, *J. Magn. Reson.* **96,** 432 (1992).
23. M. A. McCoy and L. Mueller, *J. Magn. Reson.* **98,** 674 (1992).
24. G. W. Vuister and A. Bax, *J. Magn. Reson.* **98,** 428 (1992).
25. T. Hwang, M. Garwood, A. Tannus, and P. C. M. van Zijl, *J. Magn. Reson. A* **121,** 221 (1996).
26. A. Abragam, "Principle of Nuclear Magnetism," Oxford University Press, Oxford (1961).
27. S. Zhang and D. G. Gorenstein, *J. Chem. Phys.* **105,** 5659 (1996).
28. G. Bodenhausen and D. J. Reuben, *Chem. Phys. Lett.* **69,** 185 (1980).
29. R. Tycko, A. Pines, and R. Gluckenheimer, *J. Chem. Phys.* **83,** 2775 (1985).
30. T. Fujiwara and K. Nagayama, *J. Magn. Reson.* **77,** 53 (1988).